SUBMISSION TO JOURNAL OF ROCK MECHANICS AND MINING SCIENCES

DATE: 4th May 2020

REVISED: 27th May 2021

TITLE: Field validation of a detectable, magnetic, cementitious grout for rock fracture grouting

AUTHORS: Lindsey Corson[1], Christopher Reid[2], Rebecca J. Lunn[3], Grainne El Mountassir[4], Alasdair E. Henderson[5], Kenneth Henderson[6], Arianna G. Pagano[7], Yannick Kremer[8]

POSITION AND AFFILIATIONS:

[1] Teaching Associate - Department of Maths & Statistics, University of Strathclyde, Glasgow, UK.

[2] Geotechnical Engineer, BAM Ritchies, Kilsyth, North Lanarkshire, UK.

[3] Professor - Department of Civil & Environmental Engineering, University of Strathclyde, Glasgow, UK.

[4] Senior Lecturer - Department of Civil & Environmental Engineering, University of Strathclyde, Glasgow, UK.

[5] Global Director HR Business Partnering – Civil, Royal BAM Group nv, Bunnik, The Netherlands.

[6] Divisional Director, BAM Ritchies, Kilsyth, North Lanarkshire, UK.

[7] Research Associate - Department of Civil & Environmental Engineering, University of Strathclyde, Glasgow, UK

[8]Teaching Associate - Department of Civil & Environmental Engineering, University of Strathclyde, Glasgow, UK.

CONTACT ADDRESS:

Prof Rebecca Lunn

Royal Academy of Engineering and BAM Nuttall Research Chair in Biomineral Technologies for Ground Engineering

Department of Civil & Environmental Engineering

University of Strathclyde

James Weir Building

75 Montrose Street

Glasgow

G1 1XJ

Telephone: +44 (0)141 548 3275 (Department reception)

E-mail: rebecca.lunn@strath.ac.uk

KEYWORDS: rock grouting; detectable grout; geophysical monitoring; magnetic field detection.

ABSTRACT

This paper presents the development and field-scale demonstration of a cementitious grout that enables detection in the subsurface via the addition of magnetite. Through the strategic use of a grout injection borehole and an array of monitoring boreholes for conducting pre- and post-injection magnetic surveys, combined with a geologically-based model for simulating the magnetic field anomaly, this technology can locate the post-injection magnetic grout volume within the subsurface.

A series of laboratory tests were conducted to show that the addition of Bayferrox 318M magnetite to a microfine cementitious grout does not detrimentally affect grout fluidity, penetrability, gelling, bleed and compressive strength. A magnetic grout with fluid to solid ratio = 0.7 and 15% magnetite content was then injected into a borehole interval at 40-50m depth, and changes to the magnetic field were measured within six surrounding monitoring boreholes. Field trial results show that the measured magnetic anomalies (due to magnetic grout injection) correspond well to geological features identified in a nearby site investigation borehole and that these anomalies can be detected in monitoring boreholes at a distance of 3m. By optimising the fit between model simulations of the magnetic anomaly and the field trial observations, the final geometry of the grouted rock features could be determined. Results show that grout preferentially penetrated into two coal beds and along two bedding planes that cross-cut the injection hole.

1. Introduction

Permeation grouting is carried out to fill voids in soils and to seal joints and fractures in rock, with the overall aim of improving the mechanical behaviour and/or reducing permeability (Nicholson, 2015). Grouting campaigns are a component of many engineering applications where a reduction in ground permeability is critical: (i) to minimise groundwater inflow during

construction and operation (e.g. tunnels, shafts) (ii) to ensure stability (e.g. dams), or (iii) to prevent the flow of contaminated groundwater off-site (e.g. during decommissioning of nuclear sites) (Donaldson Associates, 2012; Nicholson, 2015; Tolppanen and Syrjänen, 2003; Park and Oh, 2018; Mulligan at al., 2001; Osgoui and Unal, 2009; Liu et al., 2018). The success of a grouting operation is determined by the degree to which fractures, cavities, or pore spaces become filled with grout in order to meet pre-defined criteria, (e.g. the groundwater inflow rate to a tunnel).

Grouting campaigns in Europe often use the Grouting Intensity Number (GIN) method (Lombardi & Deere, 1993) which defines the grouting intensity as the product of the final grout pressure and the grout volume injected (per metre). The GIN value, alongside maximum values of pressure and grout take volume, are then used as cut-off criteria to control the energy applied to the subsurface and thus limit the risk of ground heave. Design of the grout injection point layout and specification of appropriate GIN values require knowledge of the grout penetration in the subsurface (Henderson et al., 2008; Rafi & Stille, 2015). At present, it is not possible to determine the extent of grout penetration in the subsurface and successful grouting remains a matter of trial and error (Tolppanen and Syrjänen, 2003; Emmelin et al., 2007). To compensate, grouting campaigns are deliberately over-designed, typically using split-spacing borehole techniques with multiple grout injections which are intended to overlap, resulting in grout wastage and the drilling of unnecessary boreholes. Without being able to detect grout in the subsurface post-injection, gaps in grout curtains may exist. Gaps may permit fluid flow, which in the case of tunnels and shafts, can cause disruption both during the construction phase and after excavations have been completed. Furthermore, gaps in the grout curtain may also remain unknown, this is of particular concern where hydraulic containment is critical to prevent contaminant migration, for example in the case of waste repositories.

Several different methods have been developed which attempt to determine the location of grout once it has been injected, including: fluorescent imaging (Chen et al., 2000), seismic monitoring (Majer, 1989), ground penetrating radar (GPR) (Zhang et al., 2010), and down-hole pH monitoring (Henderson et al., 2008). However, each method has its limitations, for example both fluorescent imaging and pH monitoring require invasive observation boreholes within the grouted rock volume which are not desirable, GPR could only detect grout at distances < 1m and in the seismic monitoring study, seismic activity could not be correlated with grout location. None of these methods are able to definitively determine the location of grout once injected into the ground.

Lunn et al. (2018) demonstrated that detection of a magnetic grout is theoretically feasible by simulating the magnetic anomaly caused by the presence of a body of magnetically-susceptible material within the Earth's magnetic field. A surface-based survey of shallow buried magnetic grout objects with a commercial magnetometer showed that the magnetic grout is detectable and good agreement was obtained between the measured and modelled magnetic anomaly. However, the research did not demonstrate that a magnetic grout could be injected into the subsurface, nor that once injected, it was detectable at depth.

In this paper, we present the development and field-scale demonstration of a grout that enables detection in the subsurface via the addition of magnetite. Through the strategic use of a grout injection borehole and an array of monitoring boreholes for conducting pre- and post-injection magnetic surveys, combined with a geologically-based model for simulating the magnetic field anomaly, this technology aims to locate the post-injection magnetic grout volume within the subsurface. The main objectives of this study were thus:

1. To investigate the influence of magnetite content on grout performance (including bleed, fluidity, penetrability, compressive strength) and magnetic susceptibility.

2. To inject magnetic grout into a borehole interval under pressure and at depth and to detect its presence using commercially available magnetometers.
3. To determine the location and geometry of the magnetic grout post-injection via numerical simulation of the magnetic anomaly in conjunction with information from the initial site investigation.

2. Magnetic Grout Characterisation

In order to create a workable grout for a permeation grouting campaign, a grout containing enough magnetite to be detectable must also have fluidity, penetrability, gelling, bleed and compressive strength characteristics comparable to those of a cement grout with no magnetic additive. In this section, the influence of magnetite content on grout performance is investigated. The materials and methods used to characterise the magnetic grouts are presented first followed by the results.

2.1 Materials and Methods

2.1.1 Grout mixes

The cement component of the magnetic grout was Spinor A12, a slag-based binder with 100% of particles <12 μm. The magnetite used was Bayferrox 318M (96.8% pure), with particles predominantly spherical and with a diameter of 0.2 μm (>95% of particles). Sikament 160, superplasticiser was used to improve fluidity and penetrability of the grout mixes and Elkem Groutaid was also used to reduce bleeding and segregation. Elkem Groutaid, consists of 50% water and 50% microsilica by mass.

Fluid to solid ratios (f/s) of 0.7, 1.4 and 2.4 were selected for investigation. 0.7 is considered as the minimum f/s ratio to produce a sufficiently fluid grout mix to ensure propagation of grout into rock fractures (Lombardi, 2003). In calculating the f/s, the mass of fluid is the sum of the mass of water, superplasticiser and half the grout aid mass used. Similarly, the mass of

solids is the sum of the mass of cement, magnetite and half the grout aid mass used. For each f/s, Spinor cement was replaced by an increasing mass of magnetite such that magnetite contents (defined as mass of magnetite/mass of cement) of 0, 10, 30 and 50% were tested. Details of the 12 grout mixes tested are presented in Table 1. Note that as the magnetite content increases at a given f/s, the water to cement ratio (w/c) increases, due to cement being replaced by magnetite.

Grout mixes 1-4 displayed an acceptably low level of bleed so no Groutaid was added to these mixes. Groutaid (%) (mass of Groutaid/mass of cement) was added to mixes with a f/s of 1.4 and 2.4 in order to achieve a grout mix with an acceptable level of bleed for use in a practical scenario. Superplasticiser content (mass of superplasticiser/mass of solids) was stepped down for the mixes at higher f/s ratios (see Table 1).

Table 1: Grout mixes tested

Grout Mix	f/s ratio	w/c ratio	Magnetite Content (%)	Groutaid Content (%)	Superplasticiser Content (%)	Specific Gravity	Cost (£/litre)
1	0.7	0.67	0	0	3.7	1.64	0.80
2	0.7	0.73	10	0	3.7	1.66	0.89
3	0.7	0.87	30	0	3.7	1.69	1.02
4	0.7	1.00	50	0	3.7	1.71	1.13
5	1.4	1.55	0	25	2.5	1.37	0.54
6	1.4	1.69	10	25	2.5	1.38	0.58
7	1.4	1.97	30	25	2.5	1.39	0.65
8	1.4	2.24	50	25	2.5	1.40	0.70
9	2.4	2.99	0	51	2.0	1.23	0.38
10	2.4	3.23	10	51	2.0	1.24	0.40
11	2.4	3.70	30	51	2.0	1.24	0.43
12	2.4	4.18	50	51	2.0	1.25	0.46

2.1.2 Grout magnetic properties

When a material is exposed to a magnetic field, how responsive the material is to becoming magnetised is called the susceptibility (Reynolds, 1997; Milsom, 2003). The magnetic susceptibility is measured by applying a known magnetic field to a sample and measuring the increased magnetism of the sample by the extra magnetic field it produces (Mussett and Khan, 2007). In this study, the volume magnetic susceptibility (χ) of the grout was measured using a Bartington MS2B susceptibility meter, χ is dimensionless. Measurements were conducted on 10ml specimens sampled from the grout mixes. Replicates were not tested in this study, as an additional study had already shown that variability in magnetic susceptibility readings for a given magnetite content is low (±0.0042) (see Supplementary Material).

2.1.3 Grout workability tests

Fluidity, expressed as the time taken for 1 litre of grout to pass through the orifice of a cone was established according to BS EN 445:2007, (British Standards Institution, 2007). In order to understand the influence of magnetite content on grout penetrability, each grout mix was investigated using the NES penetrability apparatus (Sandberg, 1997). A fixed volume of grout (1.2L) was poured into the chamber of the apparatus suspended from the ceiling via a digital weighing scale, as shown in Figure 1. The grout was injected into a slot (i.e. a mock aperture) between two parallel plates of 70 μm thickness at a pressure of 725kPa until either all of the grout had passed through the aperture or until no further efflux of grout occurred. Grout efflux was measured continuously during the test by recording the mass on the electronic scale every 5 seconds from the start of injection.

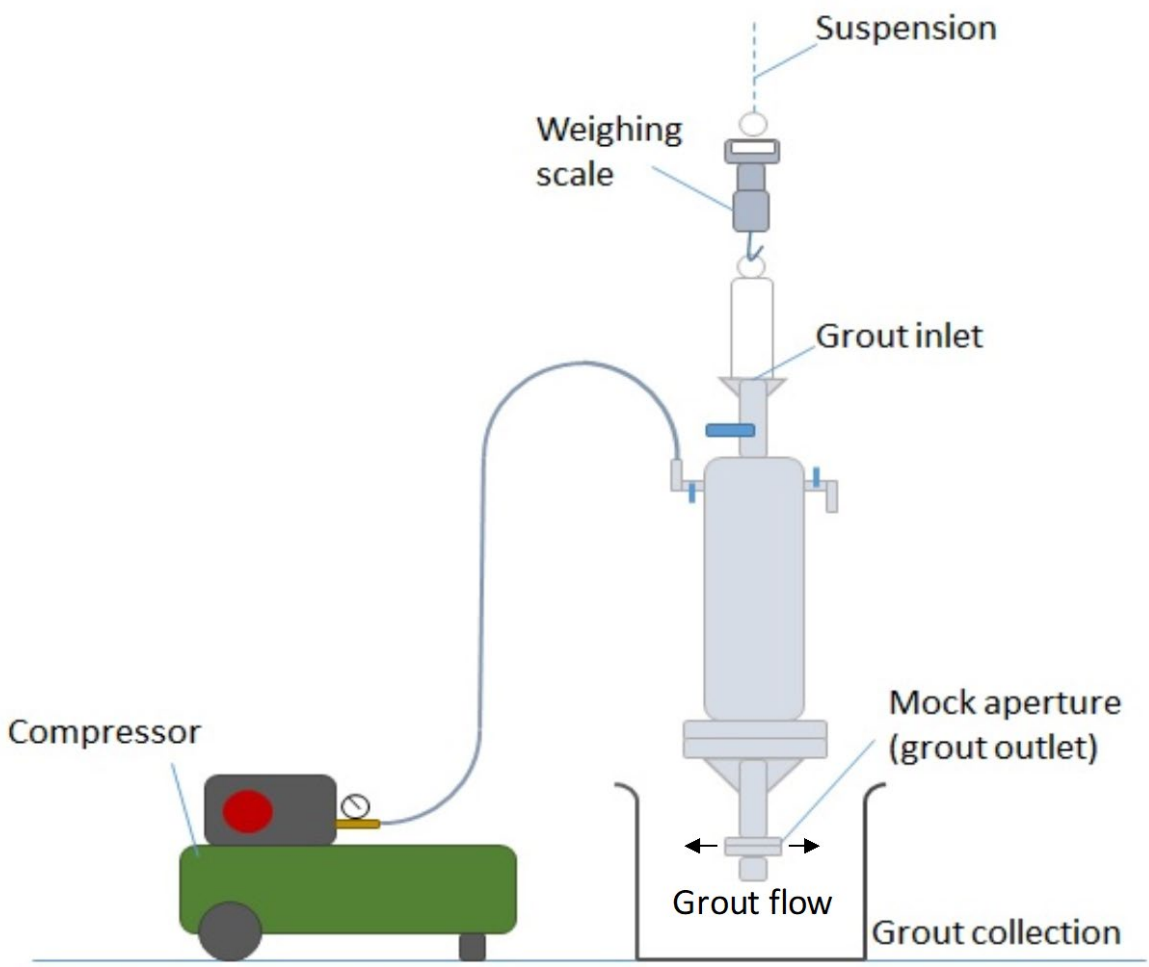

Figure 1. NES penetrability apparatus.

Gelling time was defined as the time at which no grout flows from a disposable plastic cup when filled to within 10mm of the brim and tilted to 45° (based on methods used on-site for gel tests). Grout bleed was measured according to ASTM C940 (ASTM International, 2016).

As magnetite has a high particle density (4.6 g/cm^3) compared to cement (2.94 g/cm^3) there exists the potential for magnetite particles to settle in the grout mix before the grout gels. The potential for sedimentation of magnetite within the grout was tested by pouring grout mixes 3, 7 and 11 (at 30% magnetite content) (Table 1) into 1 litre measuring cylinders. After gelling, samples were taken from the top, middle and bottom of the grout and the magnetic susceptibility of each sample measured in order to understand if there was any variation in magnetite content throughout the depth of the cylinder due to sedimentation.

2.1.4 Grout strength

Compressive strength was determined in accordance with BS EN 12390-2:2009 (British Standards Institution, 2009), with the exception that 40mm square cubic grout moulds were used instead of 100mm. This method afforded a larger data set with a limited batch size of grout. Three cubes were tested for each grout mix after 7 days curing.

2.2 Grout Characterisation Results

2.2.1 Magnetic properties

Figure 2 presents the relationship between magnetic susceptibility and magnetite content for all grout mixes in Table 1. As expected, magnetic susceptibility increases with increasing magnetite content. The relationship is not linear because the magnetite content is the mass of magnetite/mass of cement and for a given f/s, the mass of cement is decreasing as it is replaced by magnetite. Increasing f/s while keeping the magnetite content constant results in less magnetite per unit volume and hence a lower magnetic susceptibility. For example, in order to create a grout with a magnetic susceptibility of approximately 0.055 at a f/s of 0.7, a magnetite content of 10% would be required, whereas at a f/s of 2.4 50% magnetite content would be needed.

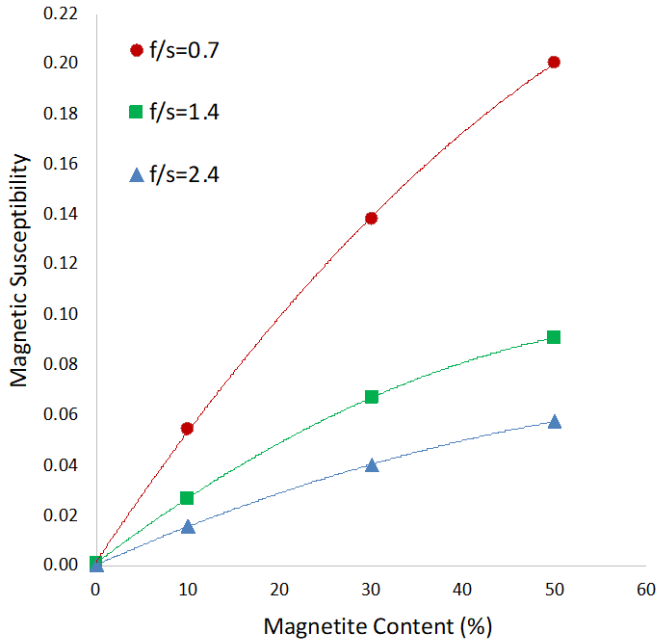

Figure 2. Influence of magnetite content and f/s ratio on magnetic susceptibility.

2.2.2 Grout workability

Figure 3 shows the effect of increasing magnetite content at constant f/s ratios on (a) grout fluidity, (b) grout penetrability and (c) grout bleed for the grout mixes listed in Table 1. Figure 3(d) plots the magnetic susceptibility at the top, middle and bottom of a gelled 1 litre grout cylinder, to investigate the potential for magnetite sedimentation.

Fluidity

The results of Marsh cone tests are shown in Figure 3(a). The equivalent fluidity of water (shown by the black cross) is also included for reference. A Marsh cone efflux time of ≤25s should be achieved in order to avoid the entrainment of air voids within grouted systems (Kamalakannan et al., 2018). Figure 3a demonstrates that this was achieved in all grout mixes tested and for each f/s ratio increasing the magnetite had no effect on the fluidity of the grout.

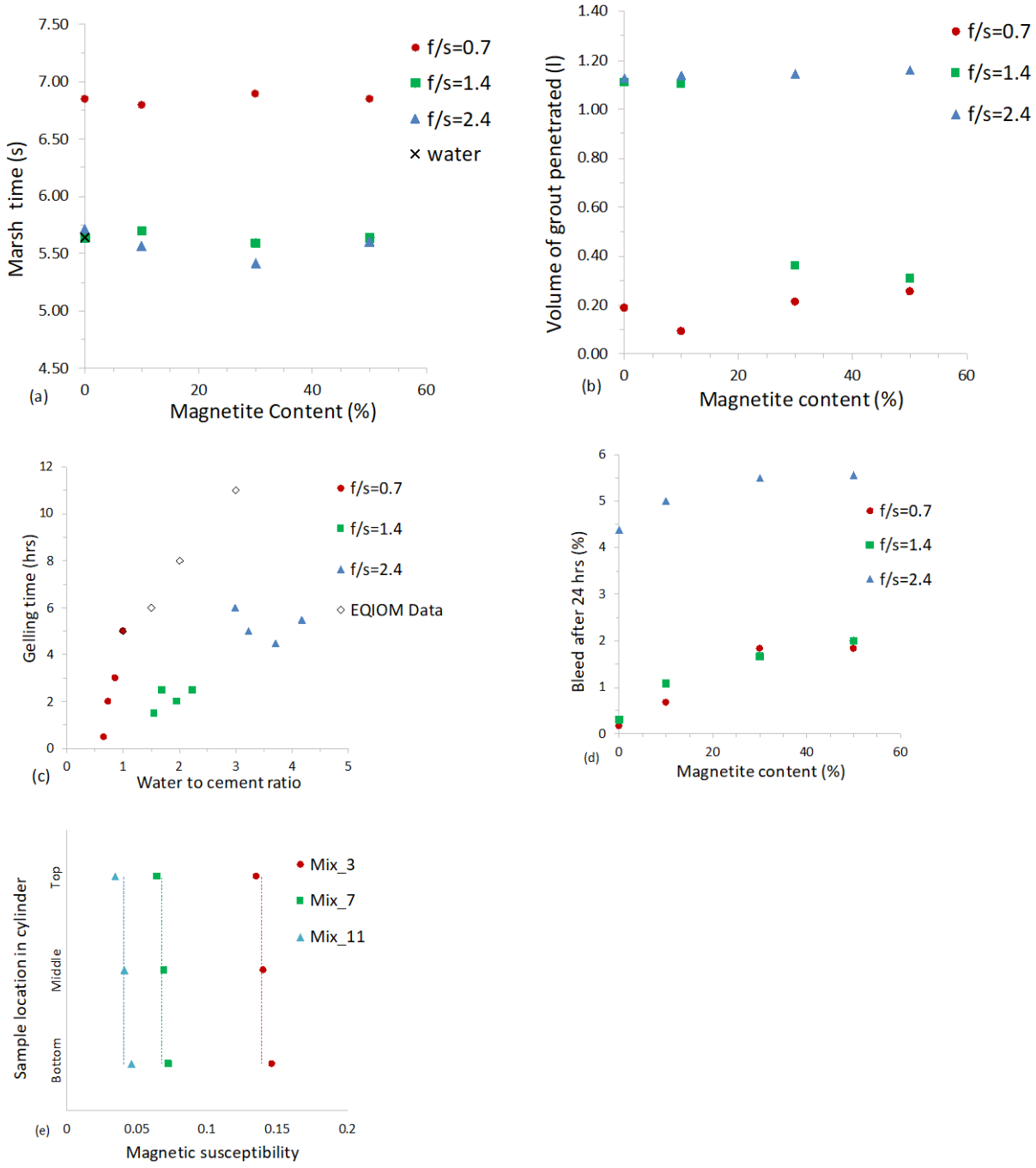

Figure 3. Influence of Magnetite content on (a) time for 1 litre of grout to pass BS marsh cone (b) total volume of grout outflow from NES apparatus (c) gelling time (d) bleed after 24 hours and (e) Magnetic susceptibility against vertical position of specimen.

Penetrability

The results of NES penetrability tests for all grout mixes are shown in Figure 3(b). For grout mixes 1-4 at f/s = 0.7, the volume of grout passing through the 70µm aperture was limited to less than 20%, with filter cakes forming in < 1minute preventing any further grout outflow. As

expected grout mixes at a f/s=2.4 (mixes 9-12) achieved a higher penetrability, with >90% of grout passing in <30s, with no filter cake formation observed. For f/s ratios of 0.7 and 2.4, increasing the magnetite content had no discernible effect on penetrability.

For mixes with f/s=1.4 at 0% and 10% magnetite, the grout exhibited high penetrability. However, as magnetite content (mass of magnetite/mass of cement) increased to 30% and 50%, penetrability of the grout reduced. This may be due to the aggregation of magnetite due to attractive forces between particles, which may not be induced at low magnetite concentrations (volume of magnetite/total grout volume) at f/s=2.4. In practice, grouts are typically mixed and therefore agitated immediately prior to injection and therefore this effect may be reduced.

Gelling time

For mixes with f/s=0/7 grout gelling times were in the range of 0.5 to 6 hours, with an increasing gel time with increasing w/c ratio (Figure 3c). Based on comparison with the manufacturer's data, specimens with and without magnetite at the same w/c ratio have the same gelling time, indicating that gelling time is not influenced by the presence of magnetite (Figure 3c). Gelling times were significantly reduced compared to the manufacturers data in mixes with f/s=1.4 and 2.4 due to the addition of varying amounts of Groutaid.

Bleed

Figure 3(d) shows that grouts with a f/s ratio of 0.7 and 1.4 (mixes 1-4 and 5-8, *Table 1*) exhibit bleed of less than 2% after 24 hours. As expected, grouts with a f/s ratio of 2.4 (mixes 9-12, *Table 1*) exhibited higher bleed ranging between 4.4% and 5.6% after 24 hours. This is despite having a higher Groutaid content (51%). A grout can be considered to be stable if it exhibits a bleed < 5% after 2hrs (Lombardi, 1985). The mixes with f/s of 0.7 and 1.4 can thus be considered stable, whereas at f/s =2.4, the 30% and 50% magnetite content mixes exceeded 5% bleed. It is possible that this could be controlled by a further increase in Groutaid content.

For each f/s ratio, increasing the magnetite content increased the bleed, this is due to the increase in the w/c ratio (see Table 1) as magnetite replaces the cement mass; this results in more water being available, which is not participating in the cement reactions.

Sedimentation

Sedimentation tests were undertaken on mixes with 30% magnetite content (mixes 3, 7 and 11). The magnetic susceptibility of samples taken from the top, middle and bottom of a 1 litre measuring cylinder after the grout had gelled was measured. This is shown in Figure 3(e) alongside the initial susceptibility of the grout mix (dashed line).

For mix 3 (corresponding to 30% magnetite at f/s = 0.7), a 3% reduction in magnetic susceptibility was determined at the top of the cylinder and a corresponding 5% increase in magnetic susceptibility at the bottom of the cylinder, indicating magnetite sedimentation did occur before grout gelling. Whereas for Mix 11, (containing 30% magnetite at f/s=2.4) a 14% reduction in magnetic susceptibility at the top of the cylinder and a 15% increase at the base of the cylinder was determined. Magnetite sedimentation was most significant at the highest f/s ratio, i.e. the lowest viscosity mix.

In practice, sedimentation of the magnetite is only an issue if a non-uniform distribution of magnetite within a grouted volume resulted in an unreliable prediction of the grouted body shape based on the anomaly it produced. In the case of fracture grouting, where discrete fractures have apertures in the μm to mm range this will not occur as (1) before injection, the grout undergoes continuous agitation ensuring an even distribution of magnetite throughout the mix and (2) after injection, sedimentation is constrained by the vertical extent of the fracture aperture.

2.2.3 Compressive strength

The results of compressive strength tests undertaken on all grout mixes are shown in Figure 4 in terms of (a) magnetite content and (b) w/c ratio. Figure 4(a) indicates that increasing the f/s

ratio reduces the compressive strength and that increasing the magnetite content also reduces the compressive strength. However, as shown in Figure 4(b), this reduction is entirely attributable to the increasing w/c ratio due to replacement of the cement mass with magnetite for a fixed f/s ratio. The data for all grout mixes are in line with the data from the manufacturer (EQIOM, Spinor datasheet) for a given w/c content. Therefore, the addition of magnetite does not influence the 7-day compressive strength, this is determined by the cement content, i.e. the magnetite itself possesses no pozzolanic reactivity nor does it negatively impact cement hydration reactions.

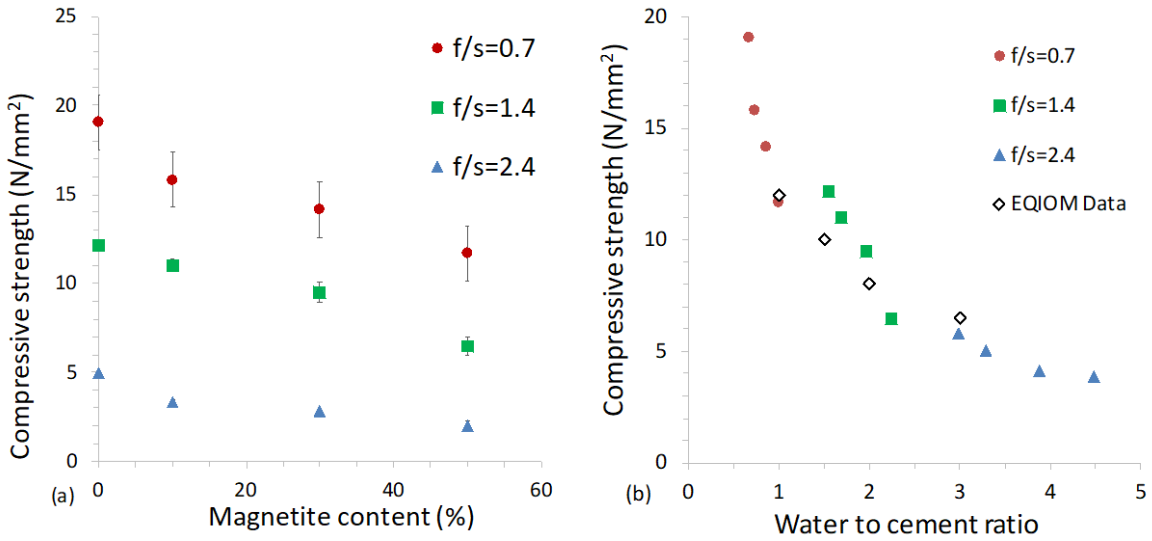

Figure 4. Compressive strength after 7 days: influence of (a) magnetite content (%) and (b) water to cement ratio.

In summary, a grout mix with a higher f/s ratio will be more fluid and hence more penetrable, increasing the likelihood of the grout achieving a greater degree of radial spread during injection and, in turn, increasing its proximity to a predetermined monitoring location. Yet a higher f/s also results in a higher bleed and a lower compressive strength. Furthermore, increasing the f/s, requires a higher magnetite content to be used in order to achieve a given magnetic susceptibility. Therefore, in practice, there is a trade-off between detectability and penetrability of the magnetic grout. For the Field Trial presented in Section 3, a f/s ratio of 0.7

was selected. The proportion of magnetite to be incorporated into the grout mix was determined based on predictions from the model presented in Lunn *et al.* (2018) which suggested a volume magnetic susceptibility, $\chi = 0.077$ would give a detectability of several metres. From Figure 2 this corresponds to a magnetite content of 15% at f/s =0.7. The magnetic remanence for this grout was determined to be 1.18×10^{-5} T using the method set forth in Schmidt and Lackie (2014).

3. Field and Modelling Methodology

3.1 Site selection

The field trial site was brownfield land which once formed part of a colliery, located in Kilsyth, Scotland (55.9709ºN 4.0864ºW). To assess the suitability of the site, a rotary cored site investigation borehole was drilled to 50.4m within which an optical televiewer survey and flow meter/spinner log measurements were performed. Overburden was found to be present to a depth of 25m, overlying horizontally interbedded fine-grained sandstone, mudstone and coal. Geological analysis of the core, shown in Figure 5, revealed a scarcity of fractures, and any fractures that were present were small and likely closed, suggesting that the geology was of low permeability. Spinner log events were recorded at depths of 35, 41.5, 43 and 47.5m, as shown by the red dots in Figure 5, indicating that fluid flow may be occurring at these depths. To assess the receptiveness of the geology to grout, standard non-magnetic grout injections were conducted over seven 3m intervals between the depths of 29.4 and 50.4m in the site investigation borehole, controlled using the Grout Intensity Number (GIN) grouting method (Lombardi & Deere, 1993). Several intervals were receptive to grout uptake. Within these intervals, grout injection was terminated when a pre-set volume control of 20l/m was achieved. On completion of these test injections, the site investigation borehole was sealed to the surface with traditional cement grout.

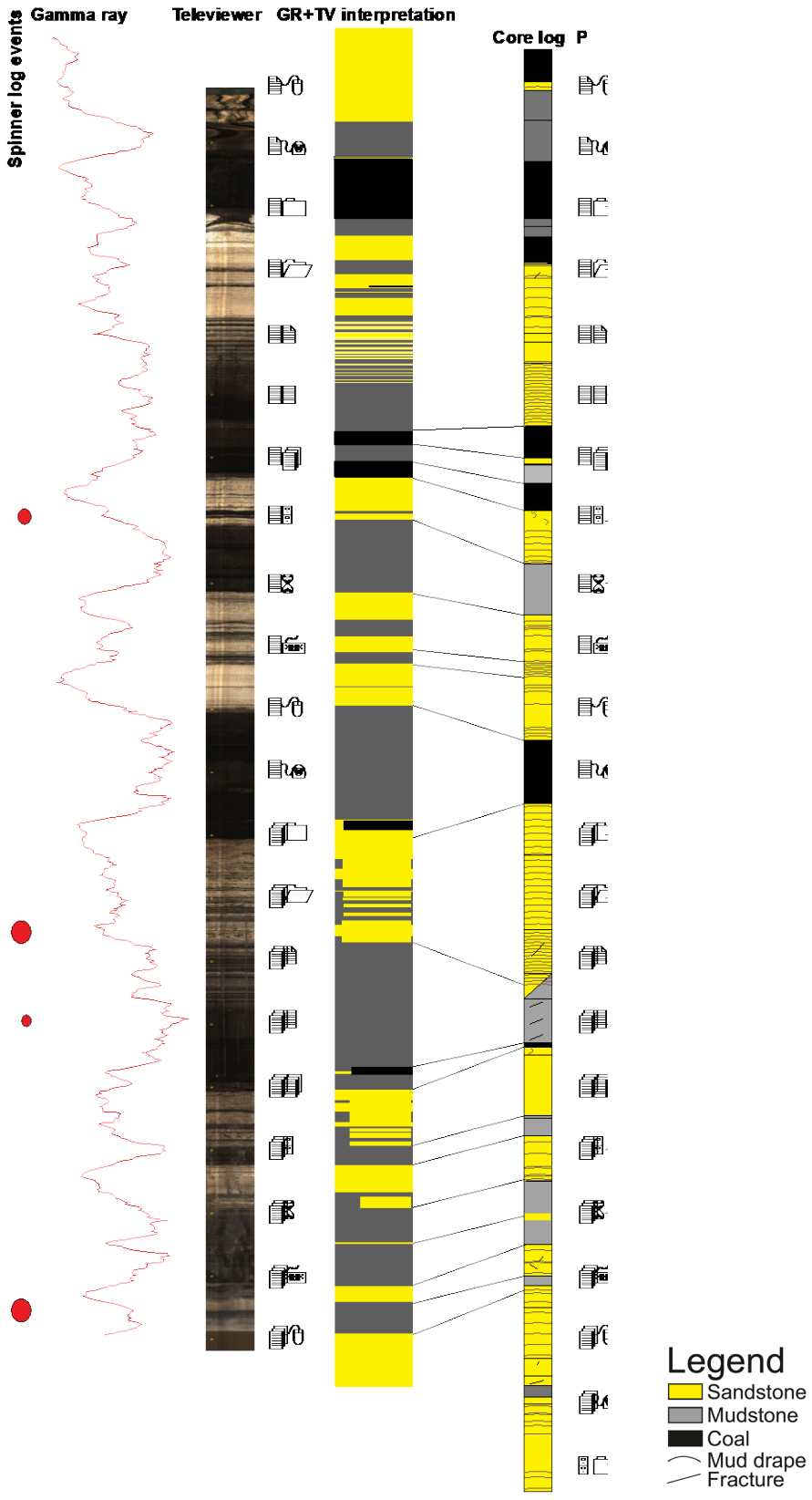

Figure 5: Results of optical borescope survey and spinner log measurements alongside interpretation of the core. In the right-hand core log yellow corresponds to regions of very fine sandstone, grey corresponds to regions of mudstone, and black regions correspond to regions of coal.

3.2 Field trial layout

Following the success of the non-magnetic injection trials into the site investigation borehole, an injection borehole and six monitoring boreholes were drilled on the site for the purposes of the field trial. These boreholes were drilled at a distance greater than 20m from the site investigation borehole so as not to affect the field trial. Figure 6 shows the plan view of the field trial borehole layout. The injection borehole (I) is centrally located with a set of three internal monitoring boreholes (M1, M3, and M5) located 1m from the injection borehole, and a set of three external monitoring boreholes (M2, M4, and M6) located 3m from the injection borehole. Each set of monitoring boreholes are equally spaced around a circle, with one borehole located to the north of the injection borehole in each set (Figure 6).

The injection borehole was drilled to 52.5m, plastic-cased to 28m, and the base was sealed to 49m with Ordinary Portland Cement (OPC). Each monitoring borehole was drilled and plastic-cased to 55m. To ensure no ingress of grout into the plastic casing during injection and to prevent potential damage to the magnetometer, the base of each monitoring borehole was sealed to 52m with OPC.

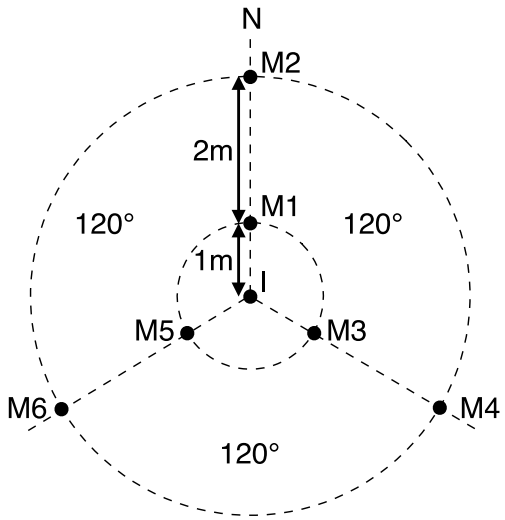

Figure 6: Plan view of the injection and monitoring boreholes.

3.3 Grout injection

The magnetic grout injected had a f/s = 0.7 and a magnetite content of 15%. Magnetic grout emplacement was split into two stages as shown in Figure 7. Stage 1 consisted of filling the bottom 3.6m of the borehole with 27 litres of magnetic grout (i.e. not injecting into the rock) via a tremie line, thus creating a 3.6m tall cylinder of grout with radius 0.05m. The purpose of this first stage was to validate the model by testing a known shape and volume of magnetic grout such that the magnetic anomalies measured in the monitoring intervals could be compared to the model predictions.

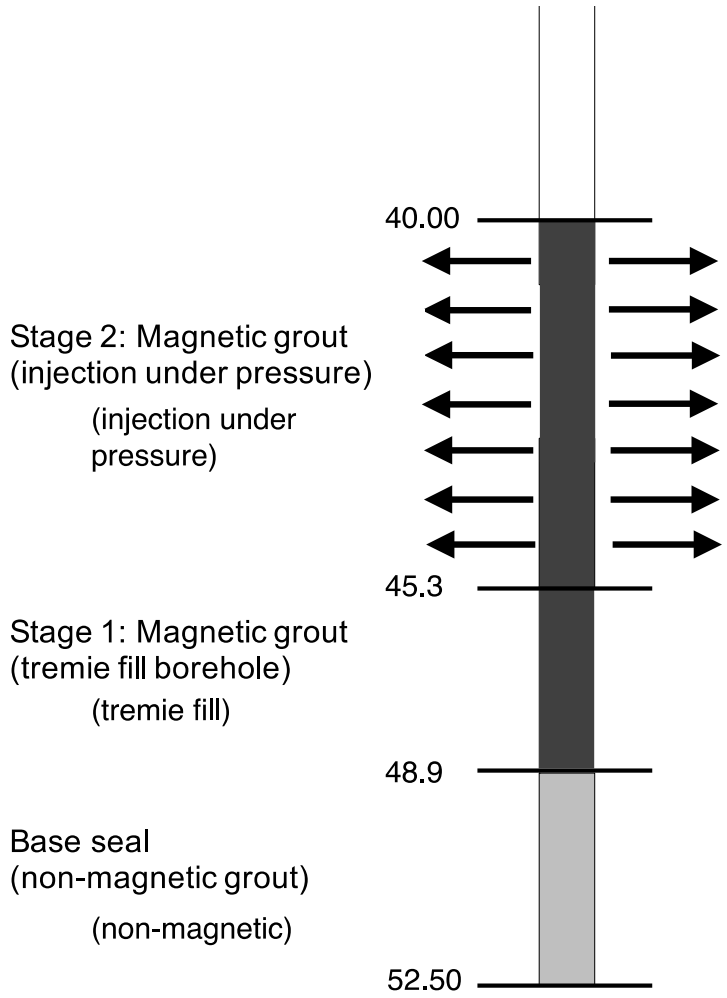

Figure 7: Schematic of the grout injection strategy. Depths measured from top of injection borehole are indicated on the left-hand side.

In Stage 2, magnetic grout was injected under pressure to achieve penetration of the grout into the rock fractures. The length of the injection interval was chosen to coincide with rock discontinuities determined from the borescope survey and spinner log events to maximise grout uptake during injection.

An inflatable packer with a grout injection line running through its centre was lowered to the base of Stage 2. The interval was primed, i.e. filled with magnetic grout under no pressure, and the packer was then extracted to the top of the interval, inflated to provide a seal against the borehole wall, and the magnetic grout was injected in two injection phases using GIN pressure and volume cut off parameters of 1400 kPa and 120 litres/m respectively. In the first phase, grout injection was terminated at 200 kPa pressure, after injecting 103 litres/m, corresponding to an injected volume of 548 litres (Figure 8(a)). In the second phase (Figure 8(b)), the remaining 77 litres of grout was injected and the injection was terminated manually. An additional 20 litres of magnetic grout topped up the interval as it drained from the injection line upon extraction of the packer. The packer was held in place after the second injection phase was complete to allow the grout to gel and avoid egression of grout from the rock mass back into the borehole.

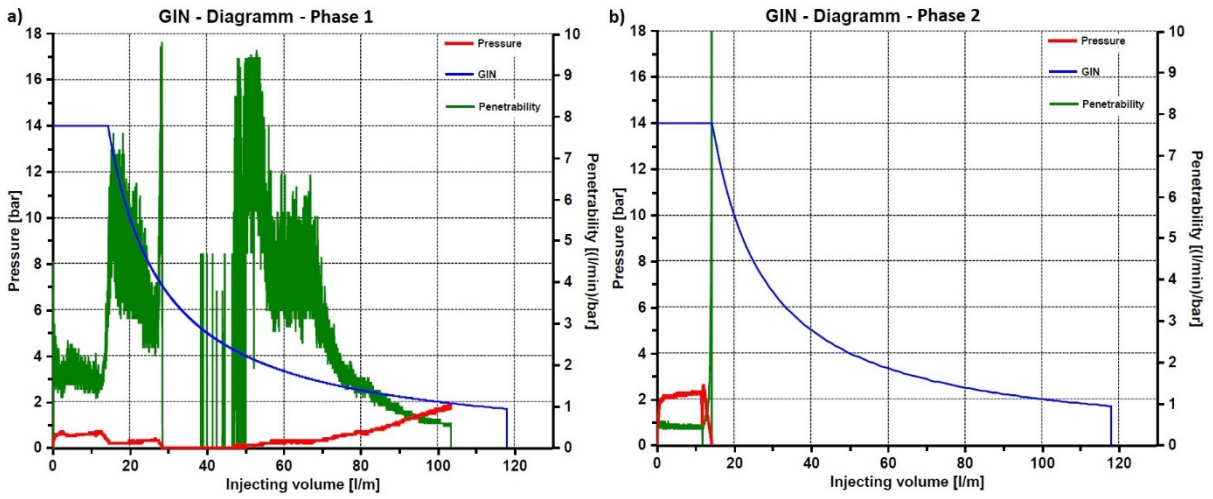

Figure 8: Grout Intensity Number (GIN) diagrams for Stage 2 (a) Phase 1, and (b) Phase 2.

3.4 Magnetic surveys

Magnetic surveys were undertaken in each of the six monitoring boreholes, before and after Stage 1 and after Stage 2, using a *Marine Magnetics SeaSpy* Overhauser effect total field magnetometer, deployed via a Geovista GV200 portable winch. The magnetometer recorded magnetic field readings at a fixed frequency, while travelling up the borehole at a constant speed, controlled via a winch. Prior to the injection of magnetic grout, in the internal monitoring boreholes (M1, M3, M5), the magnetic field was surveyed at 0.33 Hz and a winch speed of 0.4 m/min, resulting in a magnetic field measurement being obtained every 0.02m. To reduce the time taken (and hence the field trial cost) the external monitoring boreholes (M2, M4, M6) were surveyed at 0.33 Hz and a winch speed of 2 m/min, resulting in a magnetic field measurement every 0.1m. After grouting both stages, magnetic surveys were repeated in each of the six monitoring boreholes at a frequency of 0.33 Hz and a winch speed of 0.4 m/min (i.e. a resolution of 0.02m).

The marine magnetics total field magnetometer is capable of sampling at higher frequencies. However, attempts at higher frequency sampling resulted in significant noise and scatter in the data. Since, based on the field investigation borehole, the grouted fractures were likely to be of small aperture (< 2mm) it was desirable to obtain higher frequency readings. As a consequence, at the end of the field test a Bartington Mag03-MSS100 3-axis fluxgate magnetometer was obtained and trialled, with a sampling rate of 5Hz and winch speeds of 1 m/min and 2 m/min, enabling magnetic field measurements to be taken every 0.003m and 0.007m, respectively. The Bartington Mag03-MSS100 magnetometer did not exhibit increased noise at higher sampling frequencies. To prevent the 3-axis Bartington Mag03-MSS100 rotating as it was drawn up the borehole, narrower bore inclinometer casing was installed inside the existing cased monitoring holes and a bespoke magnetometer housing was designed and 3D printed to run up and down the casing grooves.

3.5 Magnetic anomaly calculations

For each monitoring borehole, four magnetic surveys were taken: before any magnetic grout injection, after Stage 1 and after Stage 2 using the lower resolution Marine Magnetics Magnetometer and one final survey after Stage 2 using the higher resolution Bartington Mag03-MSS100 3-axis fluxgate magnetometer. To determine the change in the magnetic field as a result of the grout injection, hereafter referred to as the magnetic anomaly, it was necessary to first process the data to ensure individual surveys were comparable. Two phenomena were encountered: first, the winch speed was not completely constant which caused some misalignment of the data and second, the entire survey was subject to a drift in the average magnetic field reading (perhaps due to the proximity of steel plant during instrument calibration or daily changes in the background Earth's magnetic field which varies throughout the year). As a consequence, the data were pre-processed to account for these two phenomena using the following methodology.

First, due to small variations in the winch speed, the pre- and post-grout surveys are the same shape but there is a misalignment of the peaks (Figure 9(a)) which results in errors to the depth estimation. This difference was corrected by lining up prominent troughs of the same size between each data set and linearly correcting the estimated depths in-between each pair of troughs, as shown in Figure 9(b). Second, the drift was corrected by calculating the average magnetic field over the depth range 38 – 40 m, and subtracting it from the measured magnetic field (Figure 9(c)). This depth range was chosen as it lies above the region filled with magnetic grout in stage 2, and the shape of the anomalies (peaks) were not greatly affected by the presence of the magnetic grout (see the good correspondence between pre-and post- grout surveys in the upper 4m of Figure 9(c)). Once the data were aligned and corrected for drift, the magnetic anomaly arising from the injection of magnetic grout was calculated by subtracting the magnetic field obtained in the pre-grout survey from that of the post-grout survey (Figure

9(d)). The anomaly data are noisy, even in the upper section of the borehole interval above the grout injection. As discussed earlier, this is in large part due to problems encountered with the Marine Magnetics SeaSpy magnetometer.

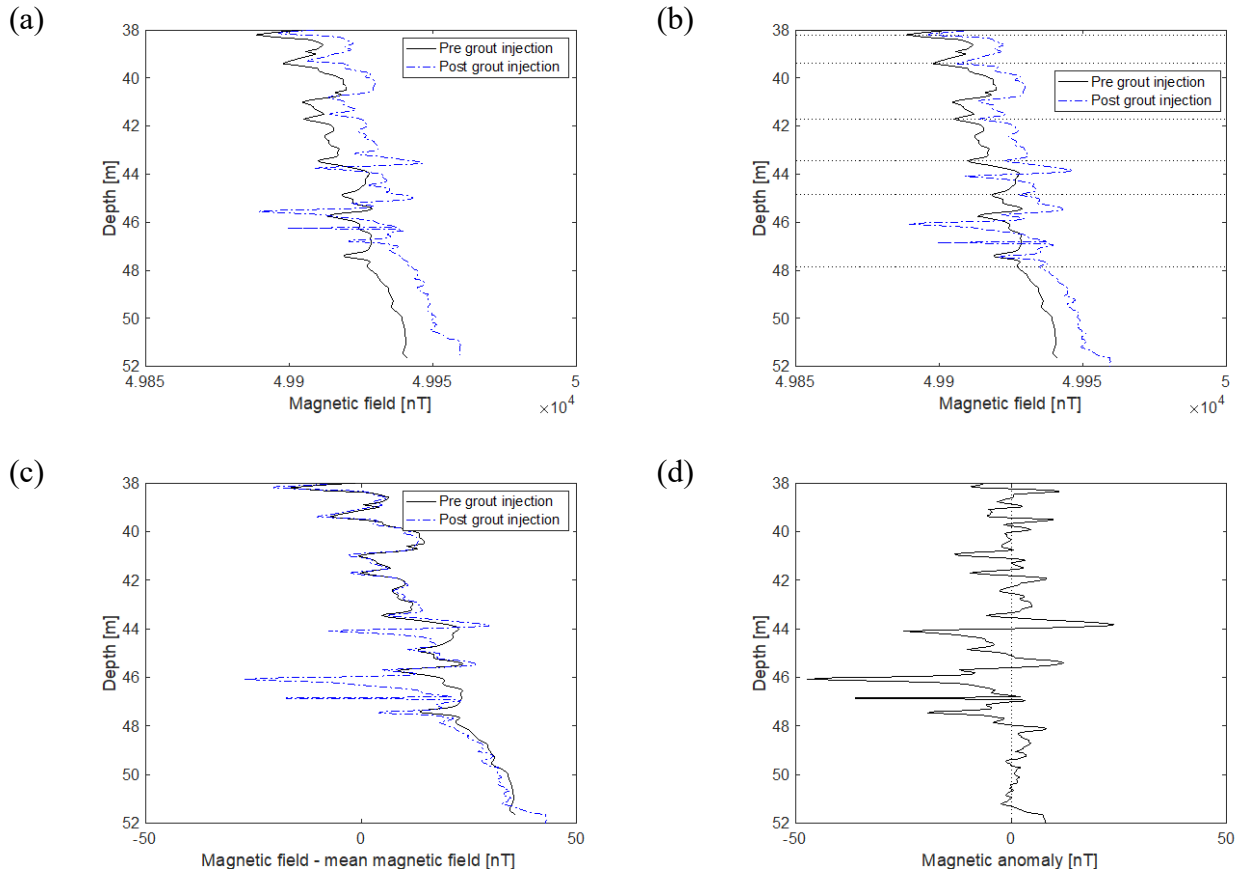

Figure 9: (a) Raw data, (b) after the correction of discrepancies between depth measurements (c) after the subtraction of the average magnetic field over 38 – 40m, (d) magnetic anomaly.

3.6 Magnetic Modelling Methodology

The theoretical and numerical model used in this research is described in Lunn *et al.* (2018), therefore only a summary is presented here. The magnetic field produced by the presence of a body containing magnetite within the ground is governed by Maxwell's magnetostatic equations:

$$\nabla \cdot (\mu(\boldsymbol{H}_b - \nabla\psi_a) + \boldsymbol{B}_r) = 0. \quad (1)$$

Here μ is the magnetic permeability, $\boldsymbol{H}_b$ is the Earth's magnetic field, $-\nabla\psi_a$ is the magnetic field which arises from the presence of the magnetic body, and $\boldsymbol{B}_r$ is the remanent magnetic flux density. The magnetic permeability can be written as $\mu = \mu_0(1+\chi)$ where $\mu_0 = 4\pi \times 10^{-7}$ Hm^{-1} is the magnetic permeability of free space, and χ is the magnetic susceptibility of the material.

The model solves Equation 1 using the freely available finite element software platform FreeFem++ (Hecht, 2012) to calculate the magnetic field in a cube that surrounds the magnetic object. On the boundary of the magnetic body, continuity of the magnetic field and continuity of the normal component of the magnetic flux density are assumed;

$$[\psi_a]_1^2 = 0, \quad (2)$$

$$[\boldsymbol{n} \cdot (\mu(\boldsymbol{H}_b - \nabla\psi_a) + \boldsymbol{B}_r)]_1^2 = 0, \quad (3)$$

respectively, where the notation $[\ ]_1^2$ represents the difference in a quantity across the boundary and **n** is the outward unit normal of the magnetic body. On the exterior boundary of the cube, the magnetic field which arises from the presence of the magnetic body is assumed to be zero;

$$\psi_a = 0. \quad (4)$$

After solving, the predicted magnetic anomaly, B_a is calculated by subtracting the total predicted pre-grout magnetic field from the total predicted post-grout magnetic field;

$$B_a = |\mu(\boldsymbol{H}_b - \nabla\psi_a) + \boldsymbol{B}_r| - |\mu\boldsymbol{H}_b|. \quad (5)$$

The model is validated in Lunn *et al.* (2018).

The model simulation domain used to simulate the field trial was a cube with edges of length 40m, the centre of the magnetic body (i.e. the injection well) was located in the centre of the cube. The size of the simulation domain was chosen to allow the magnetic anomaly to smoothly decay to zero at the outer boundary.

The Earth's magnetic field is assumed to be uniform within the simulation domain, with intensity, inclination and declination estimated using data from the British Geological Survey (BGS, 2015). The remanent magnetic flux density is assumed to be aligned with the Earth's magnetic field, since the magnetic grout cures within the Earth's magnetic field.

4. Results

4.1 Stage 1 – Grouting the borehole only

The magnetic anomalies determined from field measurements in the inner ring of monitoring holes (M1, M3 and M5), due to the Stage 1 injection (filling the borehole from 45.3m - 48.9m with a cylinder of magnetic grout) is shown by the solid black line in Figure 10. A clear response can be seen in each borehole, data for the outer holes (M2, M4 and M6) are not shown, as no anomalies were detected at a distance of 3m.

To model Stage 1, a magnetic body was placed in the center of the simulation domain which was a 3.6m tall cylinder of magnetic material with radius of 0.05m, inclined at the same angle as the injection borehole at that depth. The volume magnetic susceptibility was assumed to be $\chi = 0.077$ and the magnitude of the remanent magnetic flux density was 1.18×10^{-5} T.

Figure 10 compares the field measurements (black solid line) with the modelled magnetic anomaly for Stage 1 (red dash-dotted line) for M1, M3 and M5. The horizontal lines (Figure 10) show the location of the top and bottom of Stage 1 in each borehole. The shape of the modelled magnetic anomaly agrees well with the actual anomaly at the top of the cylinder in each borehole, however the magnitude of the peaks in M1 and M3 is underestimated. Increasing the magnitude of the remanent magnetic flux density to 2.5×10^{-5} T improved the fit, so this value of remanence was used in subsequent simulations.

At the bottom of boreholes M1 and M3, the agreement of the model to the measured data is poor. It is not clear what caused this error, but it was not observed again in Stage 2.

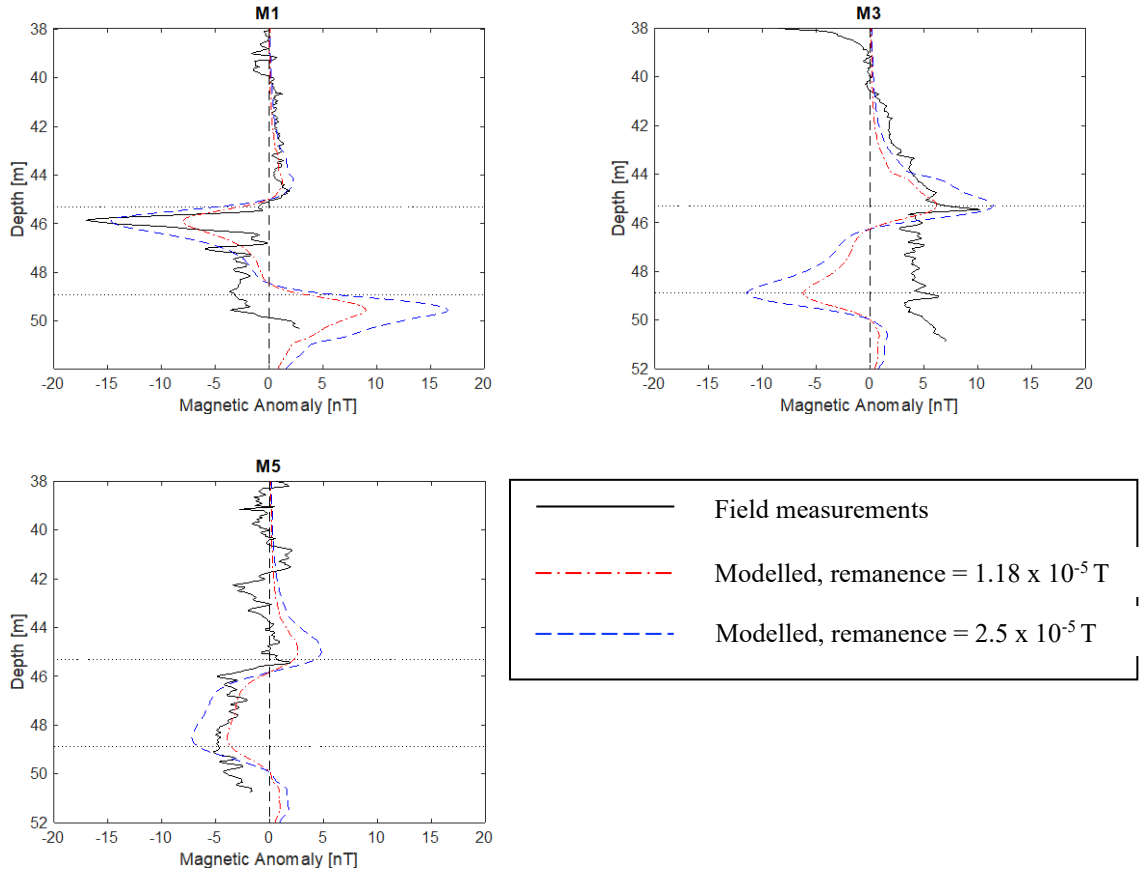

Figure 10: Comparison of magnetic anomaly determined from field measurements (black solid line) and modelled with a remanence of 1.18 x 10^{-5} T (red dash-dotted line) and 2.5 x 10^{-5} T (blue dashed line) for each of the interior monitoring boreholes (M1, M3, and M5) for Stage 1. The horizontal dotted lines indicate the location of the top and bottom of the magnetic grout cylinder emplaced in the borehole in Stage 1.

4.2 Stage 2 – Grout Injection under pressure

Figure 11(a) shows the total magnetic field obtained from the total field magnetometer (Marine Magnetics) data after injection in Stage 2. The pronounced troughs correspond to sudden decreases in the total field (approaching zero values) and were accompanied by warning messages from the magnetometer's software. These large decreases are not realistic and are attributed to the inability of the instrument to detect rapid changes in the magnetic field. Therefore, all six monitoring boreholes were resurveyed after Stage 2 injection with a Bartington Mag03-MSS100 3-axis fluxgate magnetometer. A comparison of the magnetic field obtained with both the total field and the 3-axis magnetometer is shown in Figure 11(b). Note the change of horizontal scale from (a). The pronounced troughs seen in the total field

magnetometer data correspond to more realistic smaller magnitude troughs in the 3-axis magnetometer data. Since an accurate measurement of the absolute value of the post-injection magnetic field is crucial to determining the proximity and shape of the grout front, the 3-axis Bartington magnetometer data was used.

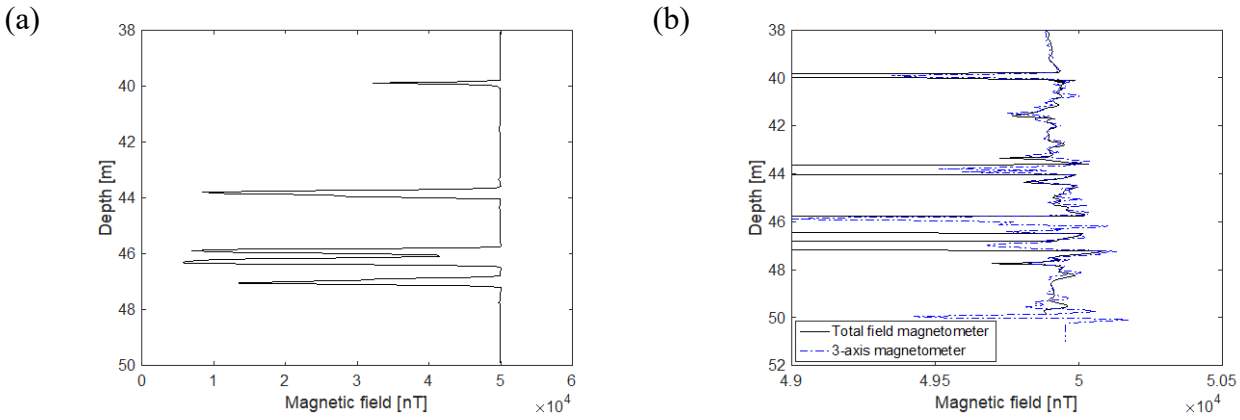

Figure 11: (a) Magnetic field plotted as a function of depth obtained from the total field magnetometer after Stage 2. (b) Comparison of the magnetic field data obtained from the total field magnetometer (black solid line) and the 3-axis magnetometer (blue dashed-dotted line) after Stage 2. Note the change of horizontal scale between (a) and (b).

Figure 12 shows the magnetic anomaly profiles estimated from the magnetic field surveys for all six monitoring boreholes. The detectability of the grout is confirmed by the presence of pronounced peaks and troughs in the magnetic anomaly profiles in each of the monitoring boreholes at 1m and 3m distance from the injection borehole. In particular, apparent in the data are four preferential paths for grout penetration that are identifiable by large anomalies in the magnetic field at depths of approximately 40m, 44m, 46m and 47m (shaded orange bands in Figure 12).

A visual comparison of the anomaly data and the geological log from the investigation borehole (Figure 5) over the same depth interval shows that the anomalies at 40m and 44m depth correspond to 1m and 0.1m thick horizontal coal beds respectively, whereas the magnetic anomalies at 46m and 47m appear to coincide with the presence of bedding planes. Hence, based on the magnetic anomaly readings, the magnetic grout has principally penetrated into

two horizontal coal beds in the upper half of the injection interval and along two bedding planes in the lower half.

A comparison of the magnitude of the anomalies between monitoring boreholes shows that grout penetration is not radial; the larger the anomaly the closer the grout front. Peak anomaly values vary significantly between boreholes for measurements at the same depth at the same radial distance from the injection hole (compare M1-M3-M5 and M2-M4-M6). For example, at 46m depth, the anomaly is greatest in M1 and M2 located to the North of the injection hole.

1

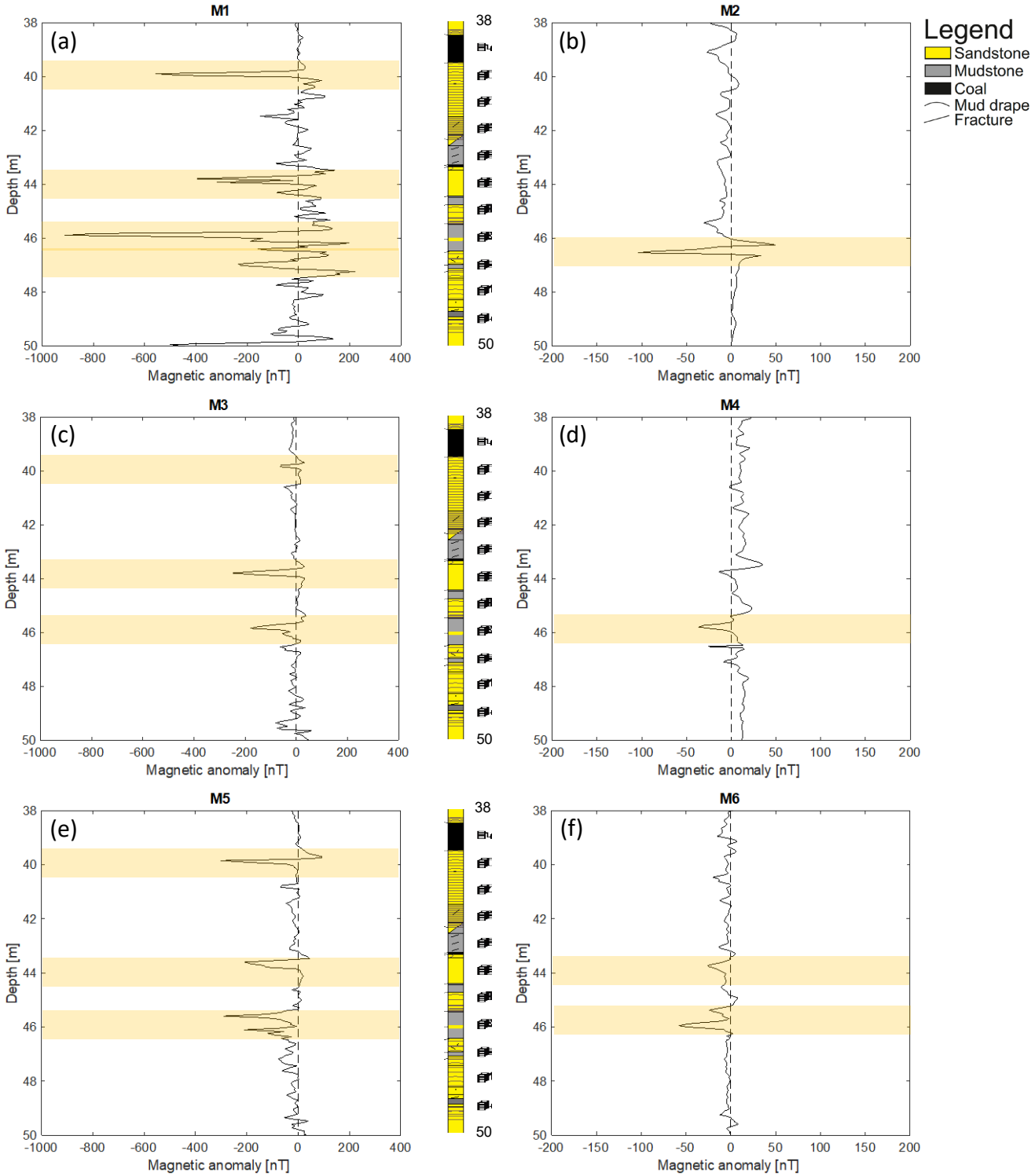

2 Figure 12: Magnetic anomaly in each monitoring borehole, alongside core log from 38m –
3 50m reproduced from Figure 5.

4 The best match between the measured and the modelled magnetic anomalies was obtained via
5 a trial-and-error procedure. The initial grout geometry consisted of a magnetic cylinder
6 representing the injection borehole, whose geometry is known, and magnetic elliptical disks

(of a given thickness) that intersect the injection hole at depths of approximately 40m, 44m, 46m and 47m, corresponding to the location of the four principal anomalies identified in Figure 12. The size, location and thickness of the elliptical disks were determined by fitting the magnitude of the magnetic anomaly: the larger the magnitude of the magnetic anomaly, the closer the edge of the magnetic disks to the monitoring borehole. The thickness of each magnetic disk was estimated by matching the width of the troughs in the magnetic data, with the maximum thickness constrained by the geological characteristics of each feature: at 40m and 44m the features were a 1m and a 0.1m wide coal band respectively, while at 46m and 47m they were two thin bedding planes, approximately 2mm thick. After each model simulation, results were compared with the magnetic anomalies measured in at least three of the monitoring boreholes at depths of 40m, 44m, 46m and 47m. Based upon the numerical results and their agreement with the measured data, a new tentative geometry was assigned for the next simulation. This trial-and-error procedure was repeated until an acceptable agreement between measured and simulated values was achieved.

Figure 13(a) shows the model results for the best-fit 3D geometry of the grouted volume. As expected, the grout spread within each geological feature is not radial, as shown in the plan view in Figure 13(b). Grout has travelled furthest in the bedding plane at 46m. For three features at 44m, 46m and 47m (the thin coal band and the two bedding planes) grout penetration is predominantly to the Northeast and Southwest, whereas in the thicker coal band at 40m depth the orientation of the preferential direction for grout penetration differs by ~ 90^{o} flowing predominantly to the Northwest and Southeast.

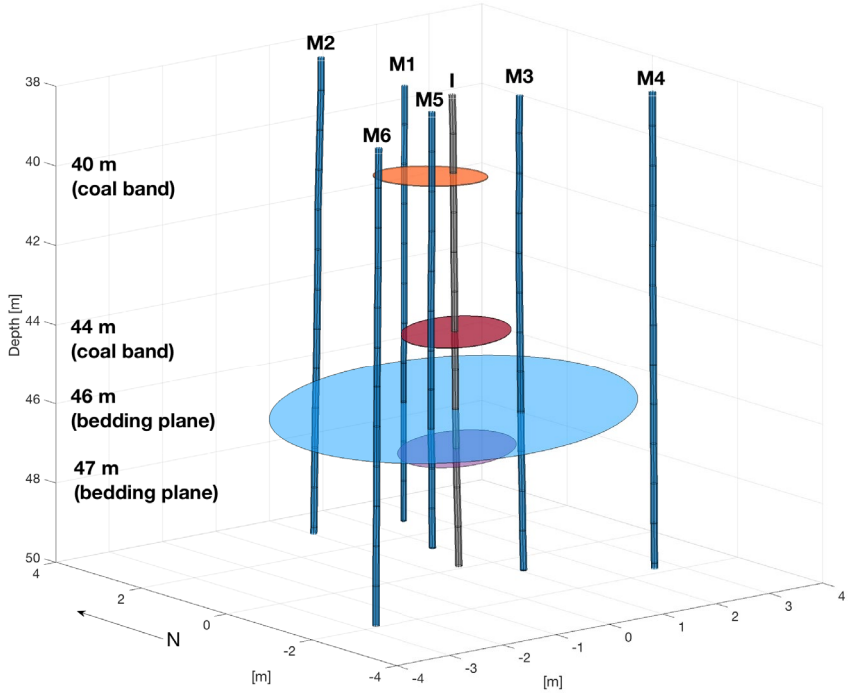

(a)

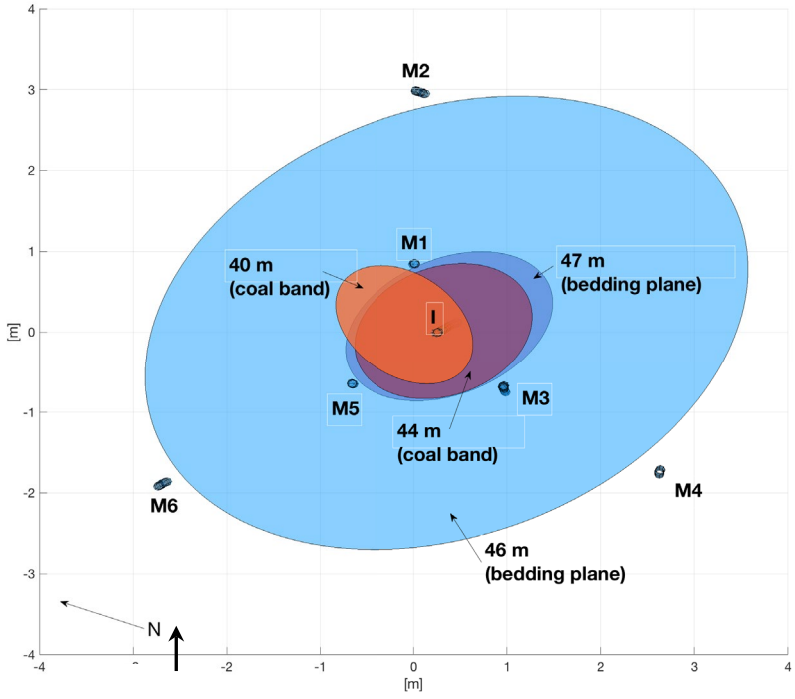

(b)

Figure 13(a) 3D view and (b) 2D plan view of the predicted geometry of the grouted volume. Note that the monitoring holes deviate slightly from the vertical and hence do not plot as points on the plan view.

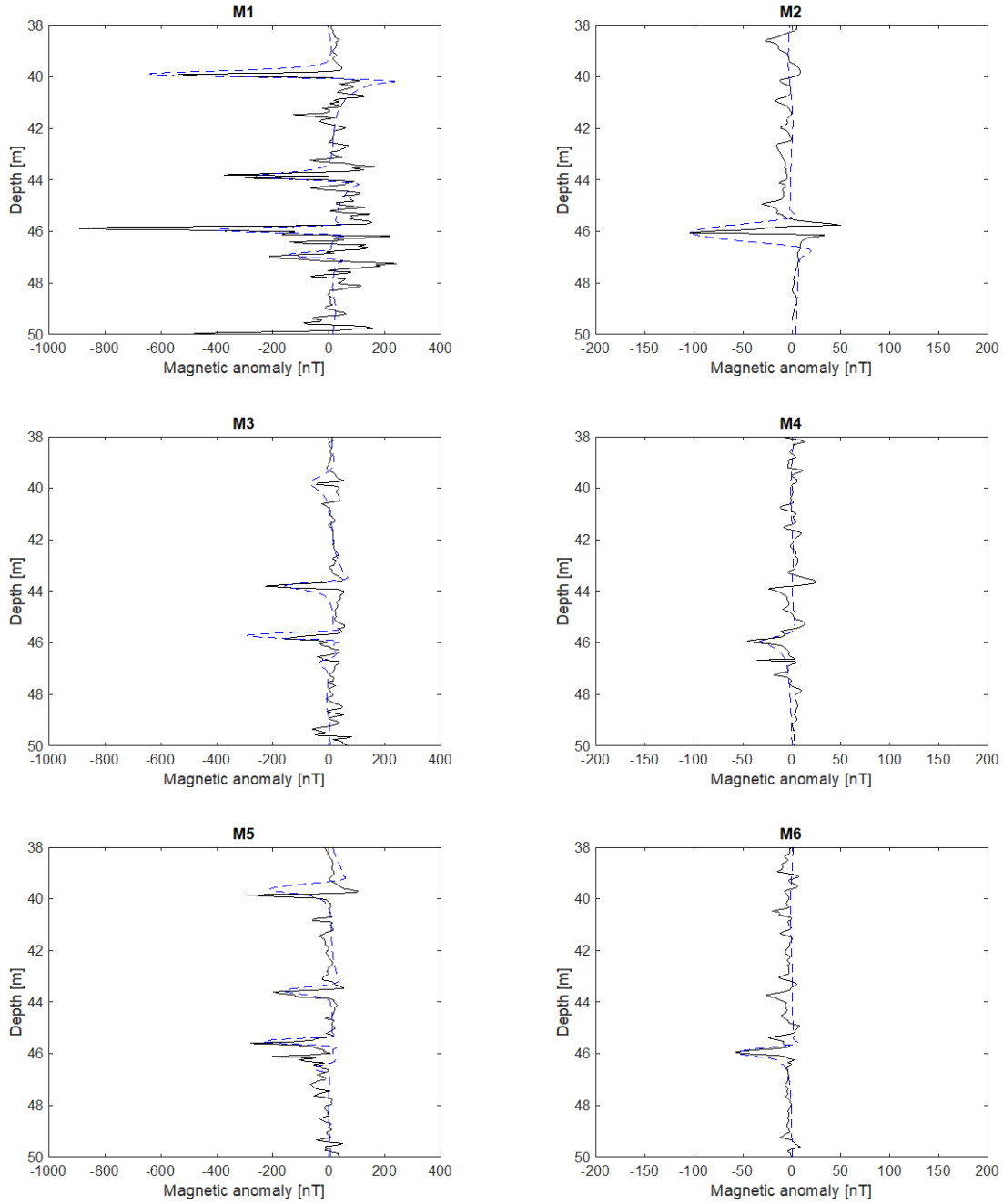

Figure 14: Comparison of actual (black solid line) and modelled (blue dashed line) magnetic anomaly for Stage 2.

Figure 14 shows a comparison between the simulated and the measured anomaly data. The four main troughs generated by the presence of injected magnetic grout are successfully captured by the model as a result of the trial-and-error procedure. The width of the troughs is related to the thickness of the feature filled by the grout i.e. the fracture aperture or in the case of the coal

beds, the combined aperture of fractures within the coal bed. For the grout that has penetrated into the two bedding planes at 46m and 47 m, 1mm, 2mm, and 3mm thick ellipses were trialled, and the width of the troughs were best fit by 2mm thick ellipses. The widths of the troughs corresponding to penetration into the coal bands at 40m and 44m were best fit by ellipses representing a combined grouted fracture thickness of 2cm and 1cm respectively.

5. Discussion

A good correspondence exists between the magnetic anomalies detected in the monitoring boreholes and the geological features identified on the borehole log, as determined from the initial site investigation borehole. Magnetic anomaly data is noisy for Stage 2, this is in part due to using a different magnetometer for the survey prior to injection of Stage 2 (Marine Magnetics Total Field Magnetometer) and post-injection of Stage 2 (Bartington Mag03-MSS100 3-axis fluxgate magnetometer). It would have been preferable to use the same magnetometer for both the pre- and post-injection surveys, however, the limitations of the Marine Magnetics Total Field Magnetometer did not become apparent until after the field trial had been conducted.

Grout has clearly been preferentially injected into the two coal seams present at the site and into two bedding plane fractures. Coal is known to form cleats (naturally occurring orthogonal joints) making it highly permeable and, therefore, able to take a significant volume of grout. A comparison of the best fit model results with the observation data for the magnetic anomalies shows that the magnitude of the anomalies is well represented and can be used to estimate the radial distance of the grout front from the monitoring boreholes. The width of each peak or trough in the anomaly data is governed by the thickness of each individual grouted feature (in individual fractures this is the fracture aperture in fractured beds, such as in the cleated coal, it is the cumulative aperture of the fractures over the bed depth) and hence can provide additional information on the geometry of the grouted rock volume. It is interesting to note that the shape

of the final grouted rock volume at this site is very different from the radially-symmetric cylindrical grouted rock volume that is traditionally assumed in commercial grouting operations. Even within individual grouted features, grout penetration is non-radial and the preferential direction of grout penetration differs by 90 degrees between some of the grouted features (Figure 13b). At this field site, no shear fractures or joints were present. In fact, the only permeability is bed parallel and the bedding is horizontal. In a more typical field setting, where joint sets are common, the grouted rock volume would be expected to take the shape of a central injection hole cross-cut by elliptical grout disks that have the same dip and strike as the open joint sets.

The deployment of magnetic grouts within routine grouting campaigns will depend both on ease of use and cost. Key will be the ability to design the layout of monitoring holes to be at sufficient distance from the grouted volume to ensure integrity of the grout curtain and to be able to reuse the monitoring holes as subsequent injection holes. The separation distance between the injection hole and monitoring holes depends on magnetic detectability. The distance over which a magnetic anomaly can be detected is determined by the volume of grout injected, the mass of magnetic material added and its magnetic properties, as well as the sensitivity of the magnetometer used, all of which can be tailored during the design process. In the field study presented, we have shown that for a separation distance of 3m between the injection borehole and monitoring holes, magnetic anomalies between 50-100nT were easily detectable. Further research is required to develop a design framework to establish the relationship between detectability over distance for variations in the grout magnetite content.

The materials cost of the magnetic cement used in the field trial is 12.5% greater than the corresponding non-magnetic cement at the same fluid to solid ratio (£0.90/litre compared to £0.80/litre). These higher material costs and costs associated with the detection system including the hiring/purchase of magnetometers are likely to be offset by costs savings

associated with a reduction in the number of boreholes drilled, and reduction in grout material used. Indeed, it may also be possible to further lower costs by only deploying magnetic grout during the initial phase of injection within a stage, such that only the grout front is magnetic, as we have shown that it is the distance to the magnetic front which controls the magnitude of the anomaly. Further research is needed to investigate the minimum duration of magnetic grout injection required within a stage while not negatively impacting on detectability.

In this study, a trial and error approach was used to infer the geometry and location of the features into which grout penetrated by comparing numerical simulations of the magnetic anomaly with those determined via field measurements. This process could be automated via the development of inversion and optimization software to enable prediction of the geometry, orientation and location of features grouted with magnetic grout. The development of such software could then enable real-time, in-situ monitoring of grout injection, providing confidence on grout curtain integrity but also enabling the design of the injection array to be reviewed as the campaign progresses.

5. Conclusions

This paper has presented the development and field-scale validation of a new detectable grouting system. The system is based on: (1) the addition of the magnetic mineral magnetite to cement grout; (2) the detection of post-injection changes in the magnetic field using magnetometers in monitoring boreholes; and (3) simulation of the magnetic data to estimate the shape and location of the grouted rock features. A series of laboratory tests were conducted to show that the addition of Bayferrox 318M magnetite to a microfine cementitious grout does not detrimentally affect grout fluidity, penetrability, gelling, bleed and compressive strength. A magnetic grout with f/s = 0.7 and 15% magnetite content was then injected into a borehole

at 40-50m depth, and changes to the magnetic field were measured within six surrounding monitoring boreholes. Field trial results showed that the measured magnetic anomalies (due to magnetic grout injection) corresponded well to geological features identified in a nearby site investigation borehole and that these anomalies could be detected in monitoring boreholes at a distance of at least 3m. By optimising the fit between model simulations of the magnetic anomaly and the field trial observations, the final geometry of the grouted rock features could be determined. Results show that grout preferentially penetrated into two coal beds and along two bedding planes that cross-cut the injection hole. Further, it is evident from the results presented here that grout penetration is non-radially symmetric and that the preferential flow direction within each grouted fracture or coal bed can differ by as much as 90 degrees between features.

This technology could revolutionise current grouting practice by reducing the uncertainty present in grouting campaigns, hence reducing costs, wastage of materials, and also the carbon footprint of grouting operations.

Acknowledgements

The authors wish to acknowledge the support of Innovate UK via the DETECTAGROUT project (Development of the first detectable permeation grouting system), Project Reference: 102066 and the support of BAM Ritchies division of BAM Nuttall Ltd.

Data statement

All data underpinning this publication are openly available from the University of Strathclyde KnowledgeBase at XXXXXXXX (DOI to be created upon acceptance of manuscript).

References

ASTM (2016) ASTM C940-16, Standard Test Method for Expansion and Bleeding of Freshly Mixed Grouts for Preplaced-Aggregate Concrete in the Laboratory, ASTM International, West Conshohocken, PA, 2016, www.astm.org. DOI: 10.1520/C0940-16.

British Geological Survey World Magnetic Model (2015) British Geological Survey, World Magnetic Model 2015 Calculator http://geomag.bgs.ac.uk/data_service/models_compass/wmm_calc.html

British Standard (2007) BS EN 445:2007. Grout for Prestressing tendons.

British Standard (2009) BS EN12390-2:2009. Testing hardened concrete Part 2: Making and curing specimens for strength tests

Chen, Y., T. Nishiyama, M. Terada, and Y. Iwamoto (2000), A fluorescent approach to the identification of grout injected into fissures and pore spaces. *Eng. Geol*., **56**, 395-401.

Donaldson Associates (2012) Pre-excavation Grouting Strategy Report. Drainage Services Department Harbour Area Treatment Scheme Stage 2A.

Emmelin, A., M. Brantberger, M. Eriksson, G. Gustafson, and H. Stille (2007), Rock grouting: current competence and development for the final repository. Stockholm: Swedish Nuclear Fuel and Waste Management Co., SKB. Report R-07-30.

EQIOM Spinor A12 Datasheet. data on Spinor A12. https://gbr.sika.com/dms/getdocument.get/a14dccff-19bf-3ed5-a173-3dfff3d4f276/Spinor_Microfine_Cement_Brochure.pdf.

Hecht, F. (2012), New development in FreeFem++. *J. Numer. Math.,* **20**, 251–265.

Henderson, A. E., I. A. Robertson, J. M. Whitfield, G. F. G. Garrard, N. G. Swannell, and H. Fisch (2008), A new method for real-time monitoring of grout spread through fractured rocks. *MRS Proc.,* **1107**.

Kamalakannan, S., Thirunavukkarasu, R., Pillai, R.G. and Santhanam, M. (2018) Factors affecting the performance characteristics of cementitious grouts for post-tensioning applications. *Constr. Build. Mater.*, **180**, pp. 681-691, doi:10.1016/j.conbuildmat.2018.05.236.

Liu, J., Chen, W., Yuan, J., Li, C., Zhang, Q., Li, X. (2018) Groundwater control and curtain grouting for tunnel construction in completely weathered granite, Bull. Eng. Geol. Environ., **77**, 515–531.

Lombardi, G. (1985). The role of cohesion in cement grouting of rock. *Proceedings of the 15th International Congress on Large Dams*, Lausanne. pp. 235-260.

Lombardi, G. & Deere, D., (1993). Grouting Design and Control Using the GIN Principle. *International Water Power and Dam Construction,* 45(6), pp. 15-22.

Lombardi, G. (2003), Grouting of rock masses. Proceedings of the third international conference on grouting and ground treatment, New Orleans, Louisiana, February 10-12, 2003. Pp. 164-197.

Lunn, R. J., Corson, L. T., Howell, C., El Mountassir, G., Reid, C., and Harley, S. L. (2018), Could magnetic properties be used to image a grouted rock volume? *J. Appl. Geophys.*, **155**, 162-175.

Majer, E. L. (1989), The application of high frequency seismic monitoring methods for the mapping of grout injections. I*nt. J. Rock Mech. Min. Sci. Geomech. Abstr.,* **26**, 249-256.

Milsom, J. (2003) Field Geophysics – The Geological Field Guide Series. Third Edition, Wiley.

Mulligan, C.N., Yong, R.N., Gibbs, B.F. (2001) Remediation technologies for metal-contaminated soils and groundwater: an evaluation, *Eng. Geol*., **60**, 193-207.

Mussett, A.E. and Khan, M.A. (2007) Looking Into the Earth: An Introduction to Geological Geophysics. Cambridge University Press.

Nicholson, P.G. (2015) *Soil Improvement and Ground Modification Methods*. Elsevier.

1 Osgoui, R.R., and Unal, E. (2009) An empirical method for design of grouted bolts in rock
2 tunnels based on the Geological Strength Index (GSI), *Eng. Geol*., **107**, 154-166.
3 Park, D., and Oh, J. (2018) Permeation grouting for remediation of dam cores, *Eng. Geol*., **233**,
4 63-75.
5 Rafi, J. Y. & Stille, H. (2015) Basic mechanism of elastic jacking and impact of fracture
6 aperture change on grout spread, transmissivity and penetrability, *Tunnelling and*
7 *Underground Space Technology,* 49 (2015) 174–187.
8 Reynolds, J.M. (1997) An Introduction to Applied and Environmental Geophysics. Wiley.
9 Sandberg P. (1997), NES-metod för mätning av injekteringsbruk inträngningsförmåga. Svensk
10 Bergs- & Brukstidning 5–6/97 (in Swedish).
11 Schmidt, P. W., and M. A. Lackie (2014), Practical considerations: making measurements of
12 susceptibility, remanence and Q in the field**.** *Explor. Geophys.*, **45**, 305-313.
13 Tolppanen, P., and P. Syrjänen (2003), Hard Rock Tunnel Grouting Practice in Finland, Sweden,
14 and Norway - Literature study. *Finn. Tunnelling Assoc.*
15 Zhang, F., X. Xie, and H. Huang (2010), Application of ground penetrating radar in grouting
16 evaluation for shield tunnel construction. *Tunn. Undergr. Space Technol.*, **25**, 99-107.